

New contributions to central exclusive production of dijets in proton-(anti)proton collisions

Rafał Maciula*

Institute of Nuclear Physics PAN, PL-31-342 Cracow, Poland

Roman Pasechnik†

*Theoretical High Energy Physics, Department of Astronomy and Theoretical Physics,
Lund University, SE 223-62 Lund, Sweden*

Antoni Szczurek‡

*Institute of Nuclear Physics PAN, PL-31-342 Cracow, Poland and
University of Rzeszów, PL-35-959 Rzeszów, Poland*

(Dated: April 3, 2024)

Abstract

We consider central exclusive production of gg dijets in proton-proton (proton-antiproton) collisions at LHC and Tevatron for different intermediate and final gluon polarisations. The amplitude for the process is derived within the k_\perp -factorization approach (with both the standard QCD and the Lipatov's effective three-gluon vertices) and is considered in various kinematical asymptotia, in particular, in the important limit of high- p_\perp jets. Compared to earlier works we include emissions of gluons from different gluonic t -channel lines as well as emission of quark-antiquark dijets. Rapidity distributions, gluon jet p_\perp distributions and invariant dijet mass distributions are presented. We explore the competition of the standard diagram with both jets emitted from a single t -channel gluon and the one with the emission from both t -channel gluons. The second mechanism requires a special treatment. We propose two different approaches. Including special kinematics and using properties of off-diagonal gluons at small x and ξ we arrive to correlations in two-dimensional distributions in rapidity of one and second jet. We find that the second contribution is much smaller than that known from the literature. The digluon production constitutes an important background to exclusive Higgs production.

PACS numbers: 13.87.Ce, 14.65.Dw

*Electronic address: rafal.maciula@ifj.edu.pl

†Electronic address: Roman.Pasechnik@thep.lu.se

‡Electronic address: antoni.szczurek@ifj.edu.pl

I. INTRODUCTION

Experimental studies of hard exclusive processes, in particular, the production of dijets at midrapidities, has been recently performed at Tevatron [1] and will be done at the LHC in the near future [2, 3].

It is expected that the contribution of the gluon pairs to the exclusive hard dijets production dominates over that from quark-antiquark pairs. Martin, Ryskin and Khoze proposed a QCD mechanism of exclusive digluon production [4]. In certain regions of the phase space, the process $pp \rightarrow p(gg)p$ (similarly to $q\bar{q}$ production) is dominated by the non-perturbative region of gluon transverse momenta, and even perturbative ingredients like the Sudakov form factor are not under full theoretical control [6]. The problem becomes even more pronounced when considering the irreducible backgrounds in central exclusive production (CEP) of Higgs boson originating from the direct exclusive $b\bar{b}$ pair production in a fusion of two off-shell gluons. In particular, in Ref. [7, 8] it was shown that the central exclusive production of $b\bar{b}$ jets at the LHC, may noticeably shadow the corresponding signal of the Higgs boson in the $b\bar{b}$ decay channel. Along with unknown NLO corrections to the k_\perp -dependent hard subprocess amplitude $g^*g^* \rightarrow jj$ (in particular, the NLO contribution from the rescattering of the final state gluons into $q\bar{q}$ pairs can be potentially important), this may lead to problems in experimental identification of the Higgs boson.

Recently, it was shown in Ref. [9] that the first LHC measurements of the exclusive dijets would significantly reduce the theoretical uncertainty for the central exclusive Higgs boson production. This makes the process under consideration especially important from both theoretical and experimental points of view.

Such a process has been recently investigated in detail in Ref. [6], and fairly good description of the Tevatron data has been achieved. We would like to extend such an analysis, both analytically and numerically, by analyzing separate contributions from different final gluon polarisations, various kinematical regions of the 4-particle phase space, which are important for future LHC measurements, and the theoretical uncertainties related with different choice of UGDs and the factorisation scale. Similarly to Ref. [6], we shall limit ourselves to the lowest-order QCD calculation, and postpone the analysis of the higher order contributions for a separate study.

Compared to the previous studies, we would like to perform an estimation of the process when one gluon is emitted from a one t -channel gluon of the QCD ladder and the second gluon is emitted from the other t -channel gluon. This contribution was discussed in Ref. [6] as potentially sizable. In this work, we present the first numerical calculation of this contribution.

Recently, the calculation of the exclusive production of quark-antiquark dijets has been performed for heavy $c\bar{c}$ [10] and $b\bar{b}$ [7, 8] pairs. Here, we extend our previous analysis and present the calculation including both contributions from light (u, d, s) and heavy (c, b) quark/antiquark jets compared to the one from the gluonic jets.

A high precision measurement of exclusive $b\bar{b}$ pair production is required for central exclusive Higgs production measurements [2, 3]. It is, therefore, instructive to estimate the reducible background for Higgs CEP at LHC coming from misidentification of gluon jets.

Another interesting point, which we would like to investigate here, is the role of the gluon reggeization in the exclusive gluonic dijets production. For this purpose, we employ the formalism of the quasi-multi-Regge kinematics (QMRK) with the Lipatov's nonlocal vertices for the triple-gluon coupling [11], and perform a numerical comparison with the

standard pQCD calculation (with standard gluons) [6].

This paper is organized as follows. In the second section, we present the standard exclusive diffractive amplitude when both gluons are produced from the same t -channel gluonic line as well as the amplitude when one of the gluons is emitted from one line and the second gluon from the second line. In the third section, we briefly remind formulae for quark-antiquark dijets with arbitrary quark mass. The fourth section contains discussion of unintegrated gluon densities and model assumptions. In the Results section, we present predictions for various differential distributions and compare our results with the available CDF data as well as discuss corresponding theoretical uncertainties. We also present predictions for future studies at LHC. Finally, the summary and conclusions close our paper.

II. DIFFRACTIVE AMPLITUDE OF THE EXCLUSIVE GLUON PAIR PRODUCTION

In this analysis, we apply the QCD mechanism for the central exclusive production, proposed by the Durham group (referred to below as the KMR approach) in Ref. [12]. In Fig. 1 we show typical contributions to the exclusive gluon pair production. In the important limit of high- p_t jets, the diagram B is suppressed by an extra hard propagator. Such a limit has been considered in detail in Ref. [6]. However, at relatively small gluon p_\perp 's, the diagram B may become sizeable and a reliable numerical estimation of its contribution is required. In this paper, for generality, we would like to calculate both contributions in all potentially interesting regions of the 4-particle phase space.

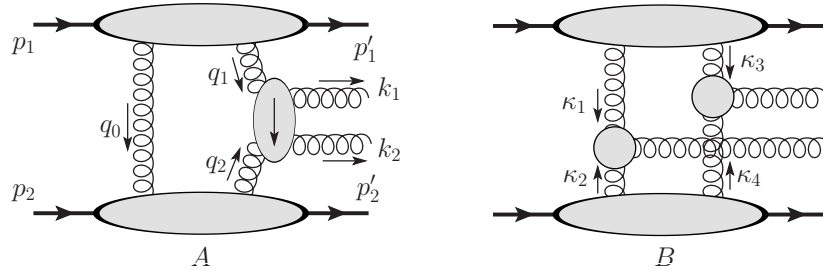


FIG. 1: Typical diagrams for the exclusive gluon pair production in exclusive double diffractive pp scattering through the gluon-gluon fusion subprocess $g^*g^* \rightarrow gg$ (A) and the 4-gluon fusion subprocess $g^*g^*g^*g^* \rightarrow gg$ (B).

Momenta of intermediate and final state gluons are given by the following Sudakov decompositions in terms of incoming protons momenta $p_{1,2}$

$$q_1 = x_1 p_1 + q_{1\perp}, \quad q_2 = x_2 p_2 + q_{2\perp}, \quad q_0 = x'_1 p_1 + x'_2 p_2 + q_{0\perp} \simeq q_{0\perp}, \quad x'_{1,2} \ll x_{1,2} \quad (2.1)$$

$$p_3 = \beta_1 p_1 + \alpha_1 p_2 + k_{1\perp}, \quad p_4 = \beta_2 p_1 + \alpha_2 p_2 + k_{2\perp}. \quad (2.2)$$

In forward scattering limit, we then have

$$t_{1,2} = (p_{1,2} - p'_{1,2})^2 = p'^2_{1/2\perp} \rightarrow 0, \quad q_{0\perp} \simeq -q_{1\perp} \simeq q_{2\perp}. \quad (2.3)$$

The Mandelstam invariants in the two-gluon fusion in the limit of high- p_\perp gluon jets $|\mathbf{k}| \equiv |\mathbf{p}_3| \simeq |\mathbf{p}_4| \gg |\mathbf{q}_0|$ can be written as [6]

$$M_{gg}^2 \equiv s_{gg} \simeq \mathbf{k}^2 \frac{(\beta_1 + \beta_2)^2}{\beta_1 \beta_2}, \quad t_{gg} \simeq -\mathbf{k}^2 \frac{\beta_1 + \beta_2}{\beta_1}, \quad u_{gg} \simeq -\mathbf{k}^2 \frac{\beta_1 + \beta_2}{\beta_2}. \quad (2.4)$$

Here and below, we use notations for the transverse 2-momenta in bold face style.

Let us first consider the explicit derivation of the diffractive amplitude shown in Fig. 1(A) as an example. Starting at the parton-level process and applying the cutting rules the imaginary part of the one-loop partonic amplitude of the gluon pair production with a fixed color indices b_1 and b_2 can be calculated in the forward limit as (for similar derivation of Higgs CEP amplitude, see Ref. [13])

$$\text{Im}M_{b_1 b_2}^{\text{parton}} = -\frac{1}{2} \cdot 2 \cdot \frac{s}{2} \frac{1}{(2\pi)^2} \cdot \tau_{im}^a \tau_{jn}^a \tau_{mk}^{c_1} \tau_{nl}^{c_2} f^{db_1 c_1} f^{db_2 c_2} \cdot (2g_s)^4 (p_1 p_2) p_{1\rho} p_{2\sigma} \cdot (ig_s)^2 \quad (2.5)$$

$$\times \int \frac{d^2 \mathbf{q}_0}{\mathbf{q}_0^2 \mathbf{q}_1^2 \mathbf{q}_2^2} dx'_1 dx'_2 \delta((p_1 - q_0)^2) \delta((p_2 + q_0)^2) \cdot \mathcal{P}_1^{\rho\nu\beta}(q_1, r_1) \mathcal{P}_2^{\beta\mu\sigma}(r_1, -q_2) \cdot \epsilon_\mu^*(\lambda_1) \epsilon_\nu^*(\lambda_2),$$

where the first factor $1/2$ comes from the cutting rule, factor 2 comes due to two identical contributing diagrams (emission of jets from the first and second t -channel gluon line), factor $\frac{s}{2} \frac{1}{(2\pi)^2}$ comes from the phase space in the loop integration, $\mathcal{P}_{1,2}$ are the effective Reggeon-Reggeon-gluon (RRG) vertices in the quasi-multi-Regge kinematics (QMRK), corresponding to the kinematical configuration with $\beta_1 \gg \beta_2$, $\alpha_1 \ll \alpha_2$ [11]. Here, we apply the eikonal approximation for the quark-gluon vertices in the proton defined by $2g_s \tau_{ij}^a p_{1,2} \delta_{\lambda\lambda'}$, where τ^a are the Gell-Mann matrices, g_s is the QCD coupling, and $\delta_{\lambda\lambda'}$ appears due to the fact that soft gluons cannot change quark helicity in an energetic proton.

For the color singlet production (since in- and outgoing protons are in the color singlet state) there is no color transfer from quark lines between protons, i.e. color indices in initial and final quarks are the same, i.e. $i = k$ and $j = l$. Then, the color averaging in each quark line leads to the substitution

$$\tau_{im}^a \tau_{jn}^a \tau_{mk}^{c_1} \tau_{nl}^{c_2} \rightarrow \frac{\delta^{c_1 c_2}}{4N_c^2}$$

in the diffractive amplitude (2.5). The appearance of $\delta^{c_1 c_2}$ here automatically gives rise to the projection of the produced gg -pair onto the color singlet state.

Further, in order to go over to the hadron level, one has to absorb the factor

$$\frac{C_F \alpha_s}{\pi} = \frac{N_c^2 - 1}{2N_c} \frac{\alpha_s}{\pi}, \quad \alpha_s = \frac{g_s^2}{4\pi} \quad (2.6)$$

into a definition of the unintegrated (q_\perp -dependent) gluon distribution function (UGDF) along each proton line as required by the underlying k_\perp -factorisation approach [13]. A reliable model for generalized off-diagonal UGDFs used in the current analysis will be discussed in some detail below.

Due to the gauge invariance and the factorisation property of the hard RRG vertices [11] we get

$$p_{1\rho} p_{2\sigma} \mathcal{P}_1^{\rho\nu\beta}(\dots) \mathcal{P}_2^{\beta\mu\sigma}(\dots) = \frac{s}{4} n_\rho^+ n_\sigma^- \mathcal{P}_1^{\rho\nu\beta}(\dots) \mathcal{P}_2^{\beta\mu\sigma}(\dots) \rightarrow \frac{s}{4} \frac{C_1^\nu(\dots) C_2^\mu(\dots)}{\mathbf{r}_1^2}, \quad r_1 = q_1 - p_3,$$

where $n^\pm = p_{1,2}/E_p^{cms}$, $E_p^{cms} = \sqrt{s}/2$, and $C_{1,2}^\mu$ are the nonlocal RRG couplings defined as [11]

$$C_1^\mu(v_1, v_2) = p_1^\mu \left(\beta_1 - \frac{2\mathbf{v}_1^2}{s\alpha_1} \right) - p_2^\mu \left(\alpha_1 - \frac{2\mathbf{v}_2^2}{s\beta_1} \right) - (v_{1\perp} + v_{2\perp})^\mu,$$

$$C_2^\mu(v_1, v_2) = p_1^\mu \left(\beta_2 - \frac{2\mathbf{v}_1^2}{s\alpha_2} \right) - p_2^\mu \left(\alpha_2 - \frac{2\mathbf{v}_2^2}{s\beta_2} \right) - (v_{1\perp} + v_{2\perp})^\mu. \quad (2.7)$$

Finally, the contributions of diagrams Fig. 1 (A) and (B) to the diffractive amplitude $\mathcal{M}^{gg} = \mathcal{M}^A + \mathcal{M}^B$ for the central exclusive gg (with external color indices a and b) dijet production $pp \rightarrow p(gg)p$ read

$$\mathcal{M}_{ab}^A(\lambda_1, \lambda_2) = is \mathcal{A} \frac{\delta_{ab}}{N_c^2 - 1} \int d^2 \mathbf{q}_0 \frac{f_g^{\text{off}}(q_0, q_1) f_g^{\text{off}}(q_0, q_2) \cdot \epsilon_\mu^*(\lambda_1) \epsilon_\nu^*(\lambda_2)}{\mathbf{q}_0^2 \mathbf{q}_1^2 \mathbf{q}_2^2} \times \left[\frac{C_1^\mu(q_1, r_1) C_2^\nu(r_1, -q_2)}{\mathbf{r}_1^2} + \frac{C_1^\mu(q_1, r_2) C_2^\nu(r_2, -q_2)}{\mathbf{r}_2^2} \right], \quad (2.8)$$

$$\mathcal{M}_{ab}^B(\lambda_1, \lambda_2) = -is \mathcal{A} \frac{\delta_{ab}}{N_c^2 - 1} \int d^2 \kappa_1 \frac{f_g^{\text{off}}(\kappa_1, \kappa_3) f_g^{\text{off}}(\kappa_2, \kappa_4) \cdot \epsilon_\mu^*(\lambda_1) \epsilon_\nu^*(\lambda_2)}{\kappa_1^2 \kappa_2^2 \kappa_3^2 \kappa_4^2} \times C_1^\mu(\kappa_1, -\kappa_2) C_2^\nu(\kappa_3, -\kappa_4), \quad (2.9)$$

where $\mathcal{A} = 2\pi^2 g_s^2 / C_F$, the minus sign in \mathcal{M}^B comes from the difference in colour factors, $f_g^{\text{off}}(v_1, v_2)$ is the off-diagonal UGDF, which is dependent on longitudinal and transverse components of both gluons with 4-momenta v_1 and v_2 , emitted from a single proton line, and

$$r_2 = q_1 - p_4, \quad \kappa_2 = -(\kappa_1 - p_4), \quad \kappa_4 = -(\kappa_3 - p_3).$$

Then the matrix element squared for the exclusive diffractive gg production cross section can be written in the standard way

$$|\mathcal{M}|^2 = \sum_{a,b} \mathcal{M}_{ab} (\mathcal{M}_{ab})^*, \quad (2.10)$$

summing up over all possible color singlet combinations of the final gluons.

The integration in the case of the emission from different t -channel gluon lines (diagram B in Fig. 1) can be made symmetric with respect to both protons by the following equivalent transformation of the integral measure

$$\int d^2 \kappa_1 \rightarrow \frac{1}{4} \int d^2 \kappa_- d^2 \kappa_+ \delta^2(\kappa_+ - \mathbf{p}_3), \quad (2.11)$$

where $\kappa_- = \kappa_1 - \kappa_2$ and $\kappa_+ = \kappa_1 + \kappa_2$ have been introduced. In practice, such a transformation is convenient in numerical calculations below.

When the p_\perp 's of the final jets are sufficiently large, the contribution of the diagram B should vanish much faster than that of the diagram A due to an extra propagator suppression in the amplitude (see Eq. 2.9). Moreover, the hard transverse momentum flow through the proton remnant would disturb it too much such that it becomes less likely to combine it back to an exclusive proton-like state after hadronisation, which should be reflected in an extra suppression by the UGDFs behavior at large gluon p_\perp . Such arguments lead to a conclusion that the diagram B can be sizeable only at relatively small jet p_\perp 's, but the large invariant mass of the gg dijet system (i.e. at large rapidity difference $\Delta y = |y_1 - y_2|$ between two jets at the edges of the central detector). Numerical estimation of such a contribution could be, therefore, important when the statistics on diffractive dijets production at LHC becomes sufficiently large. Potentially, it could even be singled out and its features could be tested if there is a region in the phase space where it may dominate.

For the emission of both gluons from the same t -channel gluon line (the standard CEP process given by diagram A in Fig. 1) we have typically: $q_{1\perp} \sim q_{2\perp} \ll p_{3\perp} \sim p_{4\perp}$. The

integration over screening gluon transverse momentum is limited to rather small $q_{0\perp} \simeq q_{1/2\perp}$ (in the forward limit).

The kinematical situation for the diagram B is different. Typically, in this case either $\kappa_{1\perp}$ is large and of the order of $p_{3\perp}$ and $\kappa_{2\perp}$ is small, or vice versa — $\kappa_{1\perp}$ is small and $\kappa_{2\perp}$ is large and of the order of $p_{3\perp}$. The integration over κ_- extends to large values, which means that typical transverse momenta of gluons in the impact factors are large. So, technically, when using grids for UGDFs we have to do it separately for both situations. Also, the kinematical structure of UGDFs are very different in diagrams A and B. This issue will be discussed in detail below.

In Eqs. (2.8) and (2.9), $\epsilon_\mu^*(\lambda_1)$ and $\epsilon_\nu^*(\lambda_2)$ are the polarisation vectors of the final state gluons with helicities λ_1, λ_2 and momenta p_3, p_4 , respectively. They can be defined in the gg rest frame with z axis along the proton beam as

$$\begin{aligned}\epsilon_\mu^*(\lambda_1) &= -\frac{1}{\sqrt{2}}(0, \lambda_1 \cos \theta \cos \psi - i \sin \psi, \lambda_1 \cos \theta \sin \psi + i \cos \psi, -\lambda_1 \sin \theta), \\ \epsilon_\nu^*(\lambda_2) &= -\frac{1}{\sqrt{2}}(0, -\lambda_2 \cos \theta \cos \psi - i \sin \psi, -\lambda_2 \cos \theta \sin \psi + i \cos \psi, \lambda_2 \sin \theta),\end{aligned}\quad (2.12)$$

such that $\epsilon^\mu(\lambda_1)\epsilon_\mu^*(\lambda_2) = -\delta^{\lambda_1, -\lambda_2}$ and $\epsilon_\mu^*(\lambda_1)p_3^\mu = \epsilon_\nu^*(\lambda_2)p_4^\nu = 0$. In this frame, momenta of protons and final-state gluons are

$$\begin{aligned}p_1^\mu &= \frac{E_1}{\sqrt{2}}(1, 0, 0, 1), & p_2^\mu &= \frac{E_2}{\sqrt{2}}(1, 0, 0, -1), \\ p_3^\mu &= E_g(1, \sin \theta \cos \psi, \sin \theta \sin \psi, \cos \theta), \\ p_4^\nu &= E_g(1, -\sin \theta \cos \psi, -\sin \theta \sin \psi, -\cos \theta),\end{aligned}\quad (2.13)$$

so that the proton and gluon energies $E_{1,2}, E_g$ and the polar angle of a gluon jet θ w.r.t. the z -axis are defined as

$$E_g \equiv \frac{\sqrt{s_{gg}}}{2} = \frac{E_1}{\sqrt{2}}(\beta_1 + \beta_2) = \frac{E_2}{\sqrt{2}}(\alpha_1 + \alpha_2), \quad \cos \theta = \frac{\beta_1 - \beta_2}{\beta_1 + \beta_2}, \quad \sin \theta = \frac{2\sqrt{\beta_1\beta_2}}{\beta_1 + \beta_2}.$$

In the high- p_\perp limit and at central rapidities of jets, the gg dijet rest frame, introduced above, becomes identical to the initial protons c.m.s. frame, which we use in actual numerical calculations below. Then the diffractive amplitude (2.8) reduces to the standard expression with $gg \rightarrow gg$ hard scattering amplitude initially derived in Ref. [6]

$$\begin{aligned}\mathcal{M}_{ab}^A &\simeq 2i\mathcal{A} \frac{s}{\mathbf{k}^2} \frac{\delta_{ab}}{N_c^2 - 1} \int d^2\mathbf{q}_0 \frac{f_g^{\text{off}}(q_0, q_1) f_g^{\text{off}}(q_0, q_2)}{\mathbf{q}_0^2 \mathbf{q}_1^2 \mathbf{q}_2^2} \sum_{\lambda_1^* \lambda_2^*} e^{i(\lambda_1^* - \lambda_2^*)\phi} \times \\ &(-2\lambda_1^* \lambda_2^*) |\mathbf{q}_1| |\mathbf{q}_2| e^{-i\lambda_1^* \phi_1 + i\lambda_2^* \phi_2} \cdot A(\lambda_1^* \lambda_2^* \rightarrow \lambda_1 \lambda_2),\end{aligned}\quad (2.14)$$

where $\phi_{1,2}$ and ϕ are the azimuthal angles of the fusing gluons $q_{1,2}$ and of the dijet production plane, respectively, λ_1^*, λ_2^* are the helicities of fusing gluons with momenta q_1, q_2 , respectively, and the nonzeroth helicity amplitudes

$$\begin{aligned}A(++ \rightarrow ++) &= A(-- \rightarrow --) = 1, \\ A(+- \rightarrow +-) &= A(-+ \rightarrow -+) = \frac{u_{gg}^2}{s_{gg}^2}, \\ A(+- \rightarrow -+) &= A(-+ \rightarrow +-) = \frac{t_{gg}^2}{s_{gg}^2},\end{aligned}$$

with Mandelstam invariants defined in Eq. (2.4), from which we see that in the QMRK limit amplitudes $A(\lambda_1^* \lambda_2^* \rightarrow \lambda_1 \lambda_2)$ reduce simply to $\delta_{\lambda_1^* \lambda_1} \delta_{\lambda_2^* \lambda_2}$. In the forward limit, provided by Eq. (2.3), we have $\phi_2 \simeq \phi_1 + \pi$, so the integral in Eq. (2.14)

$$\int d^2 \mathbf{q}_0 e^{-i(\lambda_1 - \lambda_2)\phi_1}$$

survives only when $\lambda_1 = \lambda_2$, i.e. when the gg dijet is produced in the $J_z = 0$ state, which corresponds to the well-known $J_z = 0$ selection rule in the central exclusive production processes [15]. We will discuss the subleading corrections to this rule below when presenting the numerical results for different gluon polarizations.

Below, for consistency, in order to see effects of the gluon reggeization and subleading corrections to the high- p_\perp limit we numerically compare both versions of the diffractive amplitudes – in the QMRK approximation (2.8) and in the standard approach (2.14), as well as estimate subleading contribution to the observable signal from the amplitude B with symmetric gluon couplings (2.9). The bare amplitudes above are subjected to absorption corrections which depend on collision energy and typical proton transverse momenta. We shall discuss this issue shortly when presenting our results.

III. QUARK-ANTIQUARK DIJETS PRODUCTION

Let us consider now the contribution of the quark/antiquark pairs to the observable signal of the exclusive dijets production. The hard subprocess amplitude for the $q\bar{q}$ pair production via off-shell gluon-gluon fusion was previously discussed in detail in Refs. [7, 8]. Here we would like to list the relevant formulae only, which will be used in numerical calculations below.

The amplitude of the exclusive diffractive $q\bar{q}$ pair production $pp \rightarrow p(q\bar{q})p$ reads [8]

$$\mathcal{M}_{q\bar{q}}(\lambda_1, \lambda_2) = i s \cdot 4\pi^2 \frac{\delta_{c_1 c_2}}{(N_c^2 - 1)^2} \int d^2 \mathbf{q}_0 V_{\lambda_q \lambda_{\bar{q}}}^{c_1 c_2} \frac{f_g^{\text{off}}(q_0, q_1) f_g^{\text{off}}(q_0, q_2)}{\mathbf{q}_0^2 \mathbf{q}_1^2 \mathbf{q}_2^2}, \quad (3.1)$$

Here, the vertex factor $V_{\lambda_q \lambda_{\bar{q}}}^{c_1 c_2}$ is the production amplitude of a pair of massive quark q and antiquark \bar{q} with helicities $\lambda_q, \lambda_{\bar{q}}$ and momenta p_3, p_4 , respectively. It is given by the following general expression

$$V_{\lambda_q \lambda_{\bar{q}}}^{c_1 c_2} = -\frac{2g^2}{M_{q\bar{q}\perp}^2 \sqrt{N_c}} \delta^{c_1 c_2} \bar{u}_{\lambda_q}(p_3) \left(\frac{\hat{q}_{1\perp} \hat{q}_1 - 2(p_{3\perp} q_{1\perp})}{q_{1\perp}^2 - 2(p_3 q_1)} \hat{q}_{2\perp} - \hat{q}_{2\perp} \frac{\hat{q}_1 \hat{q}_{1\perp} - 2(p_{4\perp} q_{1\perp})}{q_{1\perp}^2 - 2(p_4 q_1)} \right) v_{\lambda_{\bar{q}}}(p_4). \quad (3.2)$$

In analogy with Eq. (2.2), one can introduce the Sudakov expansions for quark momenta as

$$p_3 = x_1^q p_1 + x_2^q p_2 + p_{3\perp}, \quad p_4 = x_1^{\bar{q}} p_1 + x_2^{\bar{q}} p_2 + p_{4\perp} \quad (3.3)$$

leading to

$$x_{1,2} = x_{1,2}^q + x_{1,2}^{\bar{q}}, \quad x_{1,2}^q = \frac{m_{1\perp}}{\sqrt{s}} e^{\pm y_1}, \quad x_{1,2}^{\bar{q}} = \frac{m_{2\perp}}{\sqrt{s}} e^{\pm y_2}, \quad m_{1/2\perp}^2 = m_q^2 + |\mathbf{k}_{1/2\perp}|^2, \quad (3.4)$$

in terms of quark/antiquark rapidities y_1, y_2 and transverse masses $m_{1\perp}, m_{2\perp}$. The only difference of the quark/antiquark fractions $x_{1,2}^{q,\bar{q}}$ from that of the gluons is that they are dependent on the quark mass m_q .

It is convenient to fix the c.m.s. frame of the $q\bar{q}$ pair with z axis along the proton beam, so $\mathbf{p}_3 = -\mathbf{p}_4 = \mathbf{k}$ and $p_{3,4}^0 = M_{q\bar{q}}/2$. The gluon and quark transverse momenta (with respect to the proton beam) in the polar coordinates are then defined as

$$\mathbf{q}_{0\perp} = q_\perp(\cos\psi, \sin\psi), \quad \mathbf{p}_{3\perp} = -\mathbf{p}_{4\perp} = k_\perp(\cos\kappa, \sin\kappa),$$

respectively, and

$$k_\perp = E_q \frac{\sqrt{\gamma^2(x_1^q + x_1^{\bar{q}})^2 - (x_1^q - x_1^{\bar{q}})^2}}{x_1^q + x_1^{\bar{q}}}, \quad k_z = E_q \frac{x_1^q - x_1^{\bar{q}}}{x_1^q + x_1^{\bar{q}}}, \quad |\mathbf{k}| = \sqrt{k_\perp^2 + k_z^2} = E_q \gamma. \quad (3.5)$$

In these notations, the helicity amplitudes $g^*g^* \rightarrow q(\lambda_1)\bar{q}(\lambda_2)$ can be written as (for more detail, see Ref. [8])

$$\begin{aligned} V_{+-} = \mathcal{C} \frac{q_\perp^2}{|\mathbf{k}|} & \left[2|\mathbf{k}|q_\perp \left(|\mathbf{k}| \cos(\psi - \kappa) - ik_z \sin(\psi - \kappa) \right) + M_{q\bar{q}}k_\perp \left(k_z \cos(2\psi - 2\kappa) - \right. \right. \\ & \left. \left. i|\mathbf{k}| \sin(2\psi - 2\kappa) \right) \right] / \left[M_{q\bar{q}}^2(k_\perp^2 + q_\perp^2 + m_q^2) + 4M_{q\bar{q}}k_\perp q_\perp k_z \cos(\psi - \kappa) - \right. \\ & \left. 2k_\perp^2 q_\perp^2 (1 + \cos(2\psi - 2\kappa)) + q_\perp^4 \right], \end{aligned} \quad (3.6)$$

$$\begin{aligned} V_{++} = -2\mathcal{C} e^{-i\kappa} \frac{q_\perp^2 m_q}{|\mathbf{k}|} & \left[k_\perp^2 \cos(2\psi - 2\kappa) + |\mathbf{k}|^2 \right] / \left[M_{q\bar{q}}^2(k_\perp^2 + q_\perp^2 + m_q^2) + \right. \\ & \left. 4M_{q\bar{q}}k_\perp q_\perp k_z \cos(\psi - \kappa) - 2k_\perp^2 q_\perp^2 (1 + \cos(2\psi - 2\kappa)) + q_\perp^4 \right] \end{aligned} \quad (3.7)$$

where m_q is the quark mass, and the normalisation factor is $\mathcal{C} = 2g^2\delta^{c_1 c_2}/\sqrt{N_c}$. Below, we will use the expressions (3.6) and (3.7) in calculations of the quark jets contribution to the central exclusive dijets production at Tevatron and LHC energies of both light (u, d, s) and heavy (c, b) quarks.

IV. OFF-DIAGONAL UNINTEGRATED GLUON DISTRIBUTIONS

A. Emission from the same t -channel gluon

The off-diagonal unintegrated gluon distribution in Eq. (2.8), where longitudinal momentum fractions satisfy the strong inequality $x' \ll x$, is calculated in the forward scattering limit $q_{0\perp} \simeq q_{1/2\perp}$ according to the Kimber-Martin-Ryskin (KMR) prescription [16, 17]

$$f_{1/2g}^{\text{off}}(x_{1,2}, x', q_{1/2\perp}^2, q_{0\perp}^2, \mu^2; t) = R_g(x') \frac{d}{d \ln q_\perp^2} (x_{1,2} g(x_{1,2}, q_\perp^2) S(q_\perp^2, \mu^2))|_{q_\perp^2 = q_{1/2\perp}^2} \cdot F(t), \quad (4.1)$$

which was used e.g. in exclusive dijets studies in Refs. [9] and leads to a reasonable description of the Tevatron data [1]. In the equation above, $x_{1,2}$ and $q_{1/2\perp}^2$ are longitudinal momentum fractions with respect to the parent proton and transverse momenta squared of

the active gluons $q_{1\perp}$ and $q_{2\perp}$, respectively, $x' \sim q_{0\perp}/\sqrt{s}$ and $q_{0\perp}^2$ are the same variables for the screening gluon $q_{0\perp}$. If we assume that at small x : $xg(x) = N_g x^{\lambda_g}$ the skewedness parameter can be expressed in terms of the λ_g as [18]:

$$R_g = \frac{2^{2\lambda_g+3}}{\sqrt{\pi}} \frac{\Gamma(\lambda_g + 5/2)}{\Gamma(\lambda_g + 4)}. \quad (4.2)$$

We will take $R_g \simeq 1.2$ in practical calculations. The function $xg(x, q_\perp^2)$ in Eq. (4.1) is the collinear DGLAP gluon distribution, $S(q_\perp^2, \mu^2)$ is the so-called Sudakov form factor and the nucleon form factor in the forward limit $F(t) = \exp(bt/2)$ with the slope parameter $b \simeq 4 \text{ GeV}^{-2}$ [19] describes the coupling of the gluonic ladders to one of the nucleon lines (see Fig. 1).

The range of the integration over $d^2\mathbf{q}_0$ is formally limited by the existence of the DGLAP gluon PDF $xg(x, q_\perp^2)$. In explicit calculations we use the next-to-leading order CTEQ6 collinear distributions [20] for which $xg(x, \mu^2)$ parametrization works well down to quite small $\mu_0^2 \sim 0.4 \text{ GeV}^2$. This way we cut off the region below this starting scale μ_0^2 . This has not practical consequences for production of relatively large invariant masses as these regions are also numerically suppressed by the behavior of the Sudakov form factor for small q_\perp^2 . In order to exhibit uncertainties of our numerical results related to the collinear PDFs we also use GRV94 [21], GJR08 [22] and MSTW08 [23] distributions.

The longitudinal momentum fractions of the fusing gluons entering Eq. (4.1) are calculated as

$$\begin{aligned} x_1 &= \frac{p_{3\perp}}{\sqrt{s}} \exp(+y_3) + \frac{p_{4\perp}}{\sqrt{s}} \exp(+y_4), \\ x_2 &= \frac{p_{3\perp}}{\sqrt{s}} \exp(-y_3) + \frac{p_{4\perp}}{\sqrt{s}} \exp(-y_4) \end{aligned} \quad (4.3)$$

from the transverse momenta $p_{3/4,\perp}$ and rapidities $y_{3,4}$ of the final gluonic jets.

B. Emission from both t -channel gluons

The kinematics of the diagram B in Fig. 1 is different from that for the diagram A. Here, the off-diagonal unintegrated gluon distributions $f_g^{\text{off}}(x_1, x_3, \kappa_1^2, \kappa_3^2, \mu_1^2, \mu_2^2)$ and $f_g^{\text{off}}(x_2, x_4, \kappa_2^2, \kappa_4^2, \mu_1^2, \mu_2^2)$ should be evaluated at $x_1 \sim x_2$ and $x_3 \sim x_4$. In general, such objects are not well known and were not discussed so far in the literature. We calculate the longitudinal momentum fractions of the fusing gluons in the considered kinematical domain as follows

$$\begin{aligned} x_1 &\simeq \frac{p_{3\perp}}{\sqrt{s}} \exp(+y_3), & x_2 &\simeq \frac{p_{4\perp}}{\sqrt{s}} \exp(-y_3), \\ x_3 &\simeq \frac{p_{3\perp}}{\sqrt{s}} \exp(+y_4), & x_4 &\simeq \frac{p_{4\perp}}{\sqrt{s}} \exp(-y_4). \end{aligned} \quad (4.4)$$

As a first approximation, one could try to use a symmetric factorized prescription for the off-diagonal UGDFs, which was successfully used before for the exclusive production of χ_c mesons in Ref. [24]

$$\begin{aligned} f_g^{\text{off}}(x_1, x_3, \kappa_1^2, \kappa_3^2, \mu_1^2, \mu_2^2; t) &= \sqrt{f_g(x_1, \kappa_1^2, \mu_1^2) f_g(x_3, \kappa_3^2, \mu_2^2)} \cdot F(t_1), \\ f_g^{\text{off}}(x_2, x_4, \kappa_2^2, \kappa_4^2, \mu_1^2, \mu_2^2; t) &= \sqrt{f_g(x_2, \kappa_2^2, \mu_1^2) f_g(x_4, \kappa_4^2, \mu_2^2)} \cdot F(t_2). \end{aligned} \quad (4.5)$$

Above unintegrated diagonal distributions include Sudakov form factors in the same way as in the KMR UGDF (4.1). Since for the jet production in the diagram B $p_{3\perp} > \kappa_{1\perp}, \kappa_{2\perp}$ and $p_{4\perp} > \kappa_{3\perp}, \kappa_{4\perp}$ in most cases, so a physically reasonable choice of scales in the scale-dependent UGDFs would be $\mu_1 = p_{3\perp}$ and $\mu_2 = p_{4\perp}$ or $\mu_1 = \mu_2 = M_{jj}$. We adopt these simplest choices since we do not know the exact evolution of the Sudakov form factor in the considered kinematical domain (see, also a discussion of this issue in Ref. [6]). In this case, when the gluon q_\perp becomes bigger than the scale μ , we take simply $S(q_\perp^2, \mu^2) = 1$.

Our prescription in Eq. (4.5) does not use the fact that in the considered process both gluons are outgoing (emitted). In the collinear approach this corresponds to the ERBL kinematical region [25] where

$$|x| < |\xi|, \quad x = \frac{x_1 + x_2}{2}, \quad \xi = \frac{x_1 - x_2}{2}.$$

In our case of central dijet production typically both x_1 and x_2 are small that is also x and ξ are small. In this region the collinear off-diagonal distributions $H(x, \xi, \mu^2, t)$ can be estimated in a model independent way [18].

The discussion above suggests therefore another prescription for UGDFs in this special kinematical case:

$$f_g^{\text{off}}(x, x', k_t^2, k_t'^2, \mu^2, t) = R_{\text{coll}}(x, x'; \mu^2, t = 0) \cdot \sqrt{f_g(\bar{x}, k_t^2, \mu^2) f_g(\bar{x}, k_t'^2, \mu^2)} \cdot F(t), \quad (4.6)$$

where $\bar{x} = \frac{x+x'}{2}$, $\mu^2 = \mu_1^2 \simeq \mu_2^2$ and f_g are standard diagonal unintegrated distributions as in e.g. Ref. [16, 17]. Here R_{coll} is the ratio of collinear off-diagonal distributions in ERBL to DGLAP region:

$$R_{\text{coll}}(x_1, x_2; \mu^2, t = 0) = \frac{H_g^{\text{ERBL}}(x, \xi; \mu^2, t = 0)}{H_g^{\text{DGLAP}}(x, \xi; \mu^2, t = 0)}. \quad (4.7)$$

Assuming that at small x : $xg(x) = N_g x^{-\lambda_g}$ in the limit of small x and ξ the off-diagonal distribution $H_g(x, \xi, t)$ can be expressed in terms of λ_g as:

$$H_g(x, \xi, t) = N_g \frac{\Gamma(\lambda_g + 5/2)}{\Gamma(\lambda_g + 2)} \frac{2}{\sqrt{\pi}} \int_0^1 ds [x + \xi(1 - 2s)] \left(\frac{4s(1 - s)}{x + \xi(1 - 2s)} \right)^{\lambda_g + 1}. \quad (4.8)$$

For our estimates here λ_g is a crucial parameter which is not completely well known. In the double logarithm approximation at small values of x :

$$\lambda_g = \sqrt{\frac{\alpha_s(\mu^2)}{\pi} \log\left(\frac{1}{x}\right) \log\left(\frac{\mu^2}{\mu_0^2}\right)}. \quad (4.9)$$

However, the gluon distribution at $x < 10^{-4}$ and small factorization scales is poorly known (see e.g. a discussion in [7]). In consequence applicability of the double logarithmic formula (4.9) is not obvious and not well justified. Therefore we will treat λ_g as a free parameter. In general, it can be dependent on the scale of the problem (transverse momentum of the jet). To demonstrate uncertainties we shall show results for $\lambda_g = 0.2, 0.4, 0.6$ and 0.8 .

In Fig. 2 we show the ratio R_{coll} for different values of λ_g . The ratio strongly depends on the value. We observe a strong enhancement on the diagonal. The larger λ_g the stronger the ratio. The ratio quickly drops off diagonal. This have consequences for rapidity distributions of jets, in particular their correlations, as is discussed in the next section.

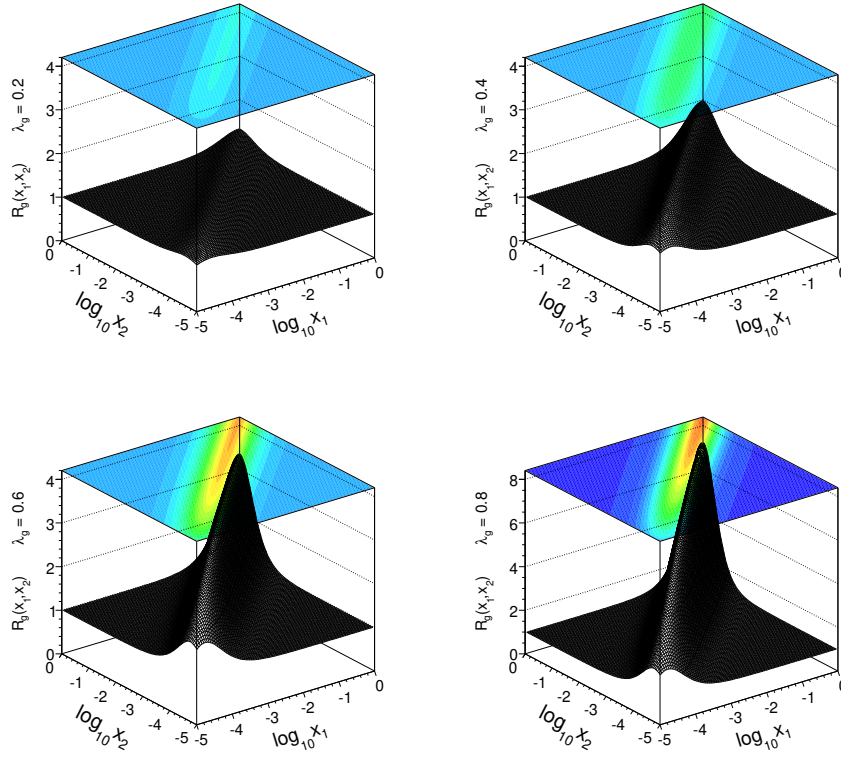


FIG. 2: The ratio from Eq.(4.7) as a function of x_1 and x_2 for different $\lambda_g = 0.2, 0.4, 0.6, 0.8$.

V. RESULTS

Let us start presentation of our results. Having the amplitude \mathcal{M} for the $pp \rightarrow p(jj)p$ where $j = g, q(\bar{q})$, defined in Eqs. (2.8), (2.9) and (3.1), we can calculate the corresponding $2 \rightarrow 4$ cross section as

$$\sigma_{pp \rightarrow pjjp} = \int \frac{d^3 p_1}{(2\pi)^3} \frac{d^3 p_2}{(2\pi)^3} \frac{d^3 p_3}{(2\pi)^3} \frac{d^3 p_4}{(2\pi)^3} (2\pi)^4 \delta^{(4)}(p_1 + p_2 + p_3 + p_4 - p_a - p_b) \overline{|\mathcal{M}_{jj}|^2}. \quad (5.1)$$

In what follows, we adopt a convenient choice of the phase space variables of the integration relevant for exclusive diffractive processes elaborated in Ref. [26].

Before we go to the description of experimental data and presentation of all contributions let us concentrate for a while on the contribution of the diagram B mechanism of hard digluon production. In Fig. 3 we show distributions of the gluonic jets in pseudorapidity and transverse momentum of the jet. The results have been performed for different values of λ_g using formula (4.6) with R_{coll} based on H_g from formula (4.8). The rapidity distribution strongly depends on the value of λ_g . The dependence is stronger for smaller transverse momenta, i.e. smaller x 's.

In Fig.4 we show similar distributions for the dijet invariant mass (left panel). There is a stronger dependence on λ_g at small invariant masses. In the region of the Higgs boson invariant mass of $M_{jj} = 120$ GeV there is a factor three uncertainties of the cross section. For comparison we show result (dashed line) obtained from a naive prescription (4.5). When the naive prescription gives large cross sections at large invariant masses the improved

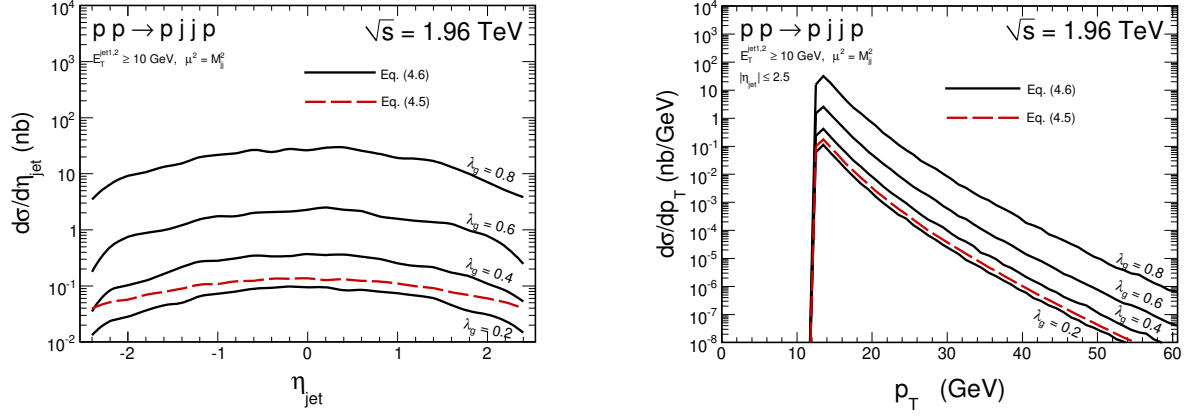


FIG. 3: Distribution in pseudorapidity (left panel) and transverse momentum (right panel) of gluonic jets for the contribution of diagram B. We present results for different $\lambda_g = 0.2, 0.4, 0.6, 0.8$. The results strongly depend on the value of λ_g . For comparison we show result (dashed line) obtained from the naive prescription (4.5).

prediction drops quickly with invariant mass. For completeness in the right panel we show distributions in rapidity difference between jets. While the distribution obtained with naive prescription extends up to large η_{diff} , the distribution obtained with improved calculations is concentrated at small values of η_{diff} .

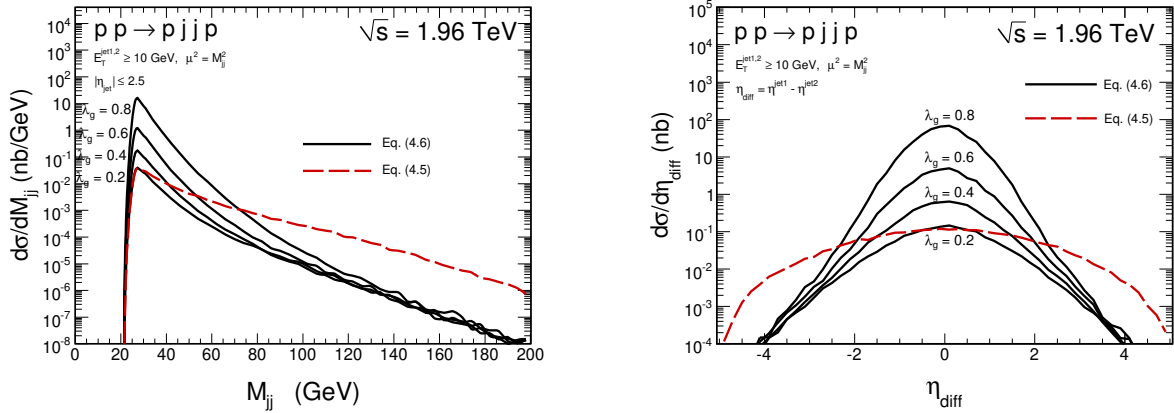


FIG. 4: Distribution in dijet invariant mass (left panel) and in pseudorapidity difference between jets (right panel) for the contribution of diagram B. We present results for different $\lambda_g = 0.2, 0.4, 0.6, 0.8$. The results strongly depend on the value of λ_g . For comparison we show result (dashed line) obtained from the naive prescription (4.5).

Now we shall include and discuss all contributions. First we shall discuss numerical results obtained at the Tevatron energy and we wish to compare our results to the existing CDF collaboration data [1]. This means that in the following we include the CDF experimental cuts. In Fig. 5 we show the integrated cross section as a function of lower cut on E_T . Following Ref. [6], we assume the relation between E_T and the jet transverse momentum p_\perp as $E_T = 0.8 p_\perp$. This approximate relation could be checked in the future by performing full simulation of jets including hadronization. We show results for the digluon diagram

A (solid curves), as well as for the diagram B (left panel, long dashed curve) and for the quark-antiquark jets (right panel, dash-dotted line). The contribution of the diagram A is somewhat bigger than presented in the literature in particular when using CHID matrix elements (left panel, short dashed line). The main reason is that in the literature (see e.g. Ref. [9]) rather large lower cuts on screening gluon transverse momentum q_\perp are imposed ($1 - 2$ GeV). Here we use gluon distributions which allow to decrease the lower cut on the gluon transverse momenta in the amplitude down to $q_\perp^{\min} \simeq 0.4$ GeV² which is consistent with the Tevatron data on exclusive production of χ_c data [24]. Having such a low cut in the case of dijets production, we rather overestimate the experimental cross section.

The contribution corresponding to diagram B turns out to be much smaller than that for diagram A known from the literature. In addition, it falls much steeper with minimal $E_{T,min}$. In the case of quark-antiquark dijets we present the contribution of $u\bar{u}$, $d\bar{d}$, $s\bar{s}$, $c\bar{c}$ and $b\bar{b}$. In the first three cases, we put the quark masses to zero, and in the last two cases we take explicit masses known from the phenomenology (1.5 GeV and 4.75 GeV, respectively). The sum of all quark-antiquark contributions is shown in the right panel by the dash-dotted curve. We conclude that the quark-antiquark jet contribution is smaller by more than two orders of magnitude than the digluon one. However, as shown in Ref. [8], the $b\bar{b}$ contribution can be essential e.g. as a background for Higgs searches in exclusive pp scattering.

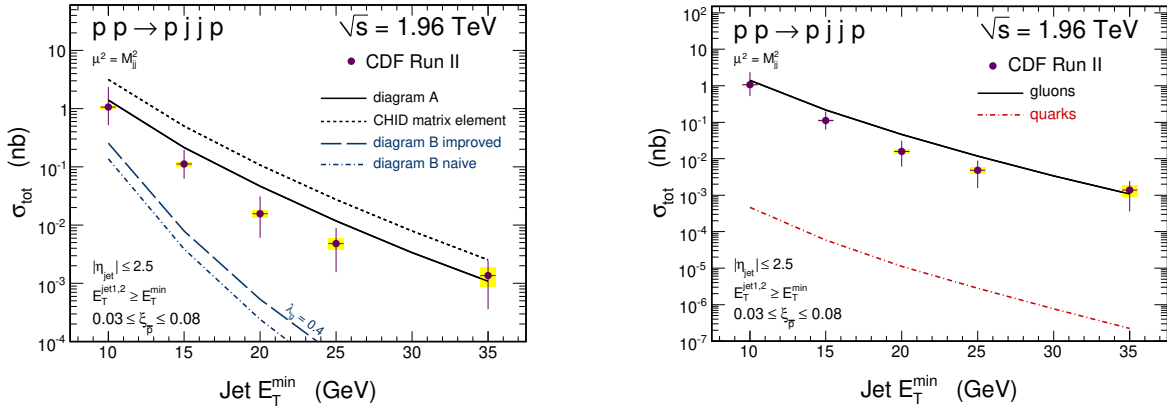


FIG. 5: The total cross section as a function of $E_{T,min}$. The experimental data points are taken from Ref. [1]. Left panel: digluon contribution for diagram A with our matrix element (solid line) and CHID matrix element (short-dashed line), for diagram B (long-dashed line). Right panel: quark-antiquark (dash-dotted line) contribution.

The exceptional dominance of digluon jets over quark-antiquark jets found here offers extraordinary conditions for increased glueball production in gluon fragmentation [27]. In order to investigate it more one needs to study a contamination of central diffractive components where the proportions of digluonic to quark-antiquark jets are less favourable.

Similarly to Ref. [9], we present model uncertainties due to the choice of PDF (Fig.6) and due to the choice of the scale ($\mu_F = \mu_R$) in the left panel of Fig. 7 for jet E_T^{\min} dependence and for dijet mass distribution in the right panel where we show separately uncertainties for diagram A and B. We observe that they are much smaller for diagram B. In the latter case the lower curve corresponds to $\mu^2 = M_{jj}^2$ and the upper curve corresponds to $\mu^2 = (p_{3\perp}^2 + p_{4\perp}^2)/2$. The smaller uncertainty for diagram B can be explained as follows. The gluon propagators cause that in a typical situation when two gluons coming from the same proton line are

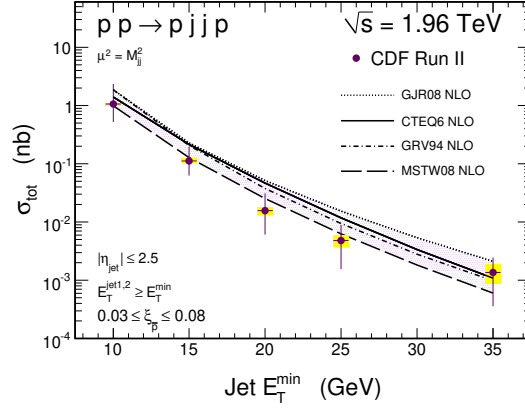


FIG. 6: Uncertainties due to the choice of PDF.

hard and the other two are soft. This is different compared to diagram A where typically all gluons are rather soft (or semi-hard).

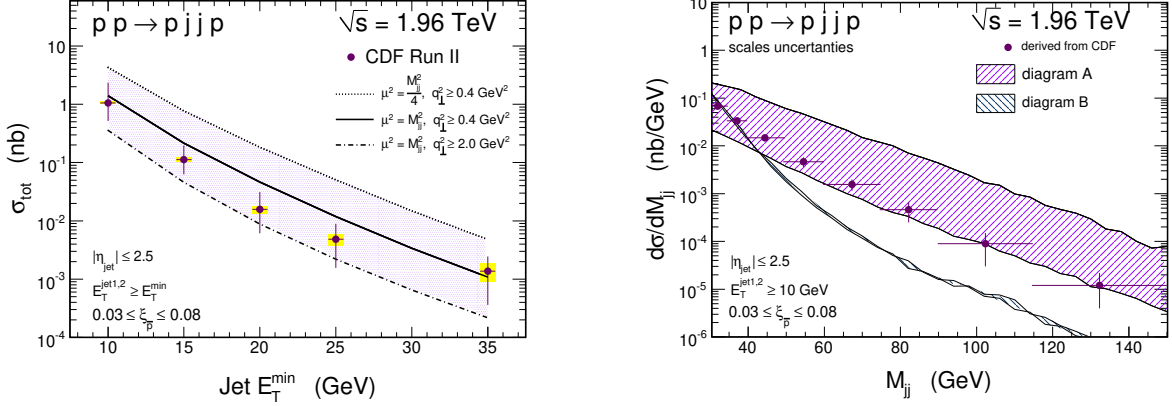


FIG. 7: Uncertainties due to the choice of the scales. Left panel: jet E_T distribution for diagram A, right panel: invariant mass distributions for both diagrams. Details are explained in the text.

In Fig. 8 we show pseudorapidity distributions of one of the gluonic jets (left panel) and distribution in jet pseudorapidity difference (right panel) for the fixed lower cut on E_T . The distribution for naively calculated diagram B is flatter than that for diagram A. The same is true in rapidity difference where the two contributions are almost identical for large rapidity differences where, however, the cross section is rather small. The corresponding distributions for improved method for calculation of diagram B are quite different than those for naive calculation. The contribution of quark-antiquark jets (dash-dotted curve) is negligible. The rapidity distributions were not presented by the CDF collaboration in Ref. [1].

In the left panel of Fig. 9 we show in addition the corresponding distributions in jet transverse momentum. The contribution of diagram B becomes negligible at large jet transverse momenta (or transverse energy). In the right panel we show the distribution in dijet invariant mass. At large invariant masses, naive calculations of diagram B give cross sections which are similar to the leading contribution from diagram A. However, the contribution of diagram B from improved prescription is sizeable only at small invariant masses and does

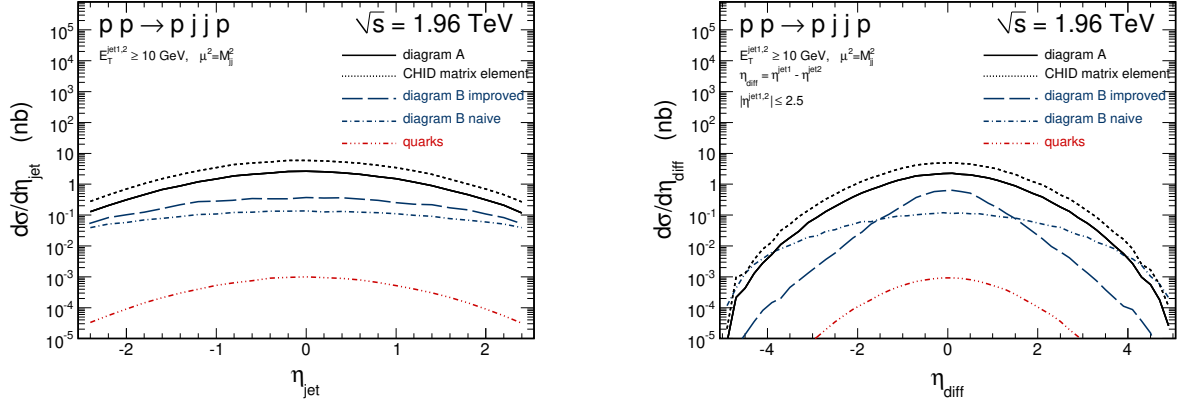


FIG. 8: The distribution in jet pseudorapidity (left panel) and in pseudorapidity difference (right panel).

not have any meaning in the important for Higgs searches large M_{jj} region.

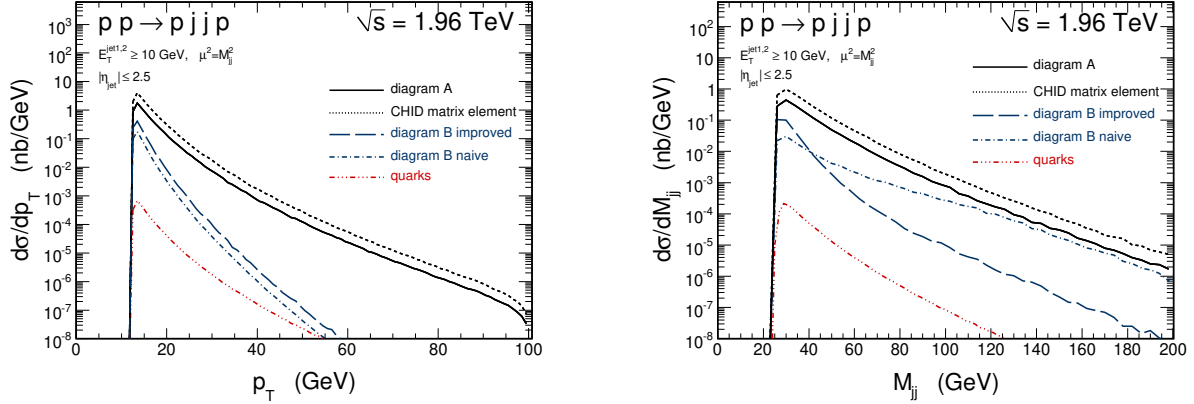


FIG. 9: The distribution in jet transverse momentum (left panel) and in dijet invariant mass (right panel).

In Fig. 10 we show separately contributions for different helicity combinations. Being fully consistent with the $J_z = 0$, we see the dominance of the $++ = --$ contributions over $+- = -+$ ones. However, our helicities are in the proton-proton center-of-mass system so the relation to the $J_z = 0$ rule is only approximate and strictly valid in the high- p_\perp jets limit.

We show similar distributions at nominal LHC energy $\sqrt{s} = 14$ TeV in Fig. 11 and 12. The situation is qualitatively similar as for the Tevatron case. Here the distributions in jet transverse momentum and dijet invariant mass are somewhat flatter. At the LHC energy, the contribution of diagram B is much smaller than for diagram A in the whole range of kinematical variables considered here.

Finally, we wish to discuss correlations in rapidity between gluonic jets. In Fig.13 we show distribution for diagram A (left panel), naively calculated contribution of diagram B (middle panel) and contributions of diagram B calculated as proposed above (right panel).

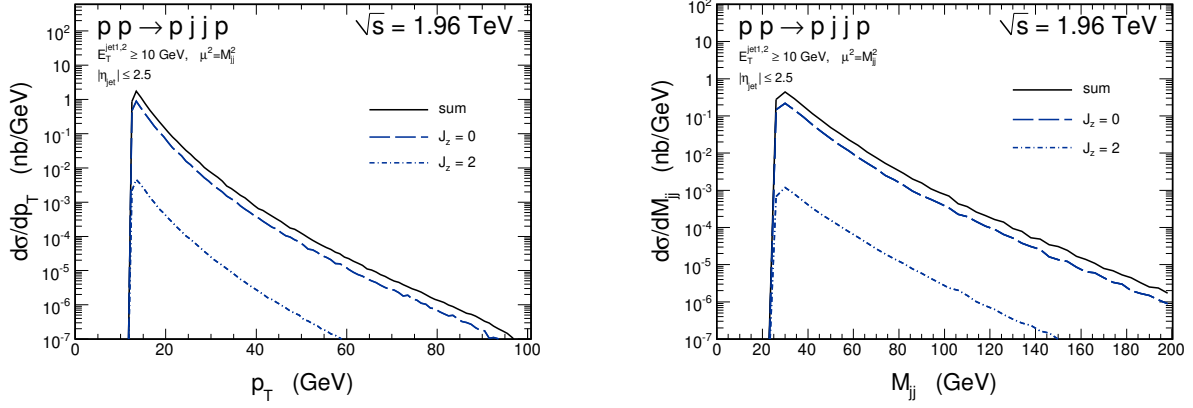


FIG. 10: The distribution in jet transverse momentum (left panel) and in dijet invariant mass (right panel) for different dijet helicity states. Only diagram A is included here.

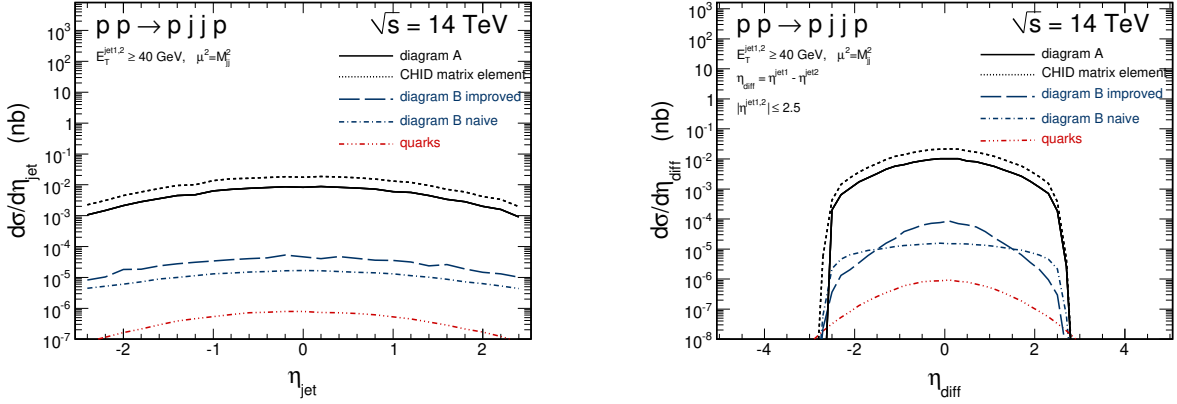


FIG. 11: The distribution in jet pseudorapidity (left panel) and in pseudorapidity difference (right panel).

The correlation for the first and second case is similar. The two gluonic jets are only weakly correlated in these variables. It is completely different for the contribution of diagram B calculated using the ratio of collinear off-diagonal gluon distributions (see Eq.(4.7)). We observe a strong ridge along the diagonal $y_3 = y_4$. This ridge is a consequence of the ratio defined in Eq.(4.7).

In Ref.[7] we have studied in detail irreducible exclusive $b\bar{b}$ background to exclusive Higgs boson production. The gluonic jets can be misidentified as b -quark jets [28]. If both gluonic jets are misidentified then such a misidentified event can contribute to a background to exclusive Higgs boson production. In Fig.14 we illustrate the situation. We show both the Higgs signal (hatched area) including experimental resolution [29, 30] as well as diffractive $b\bar{b}$ continuum, QED $b\bar{b}$ continuum as well as formally reducible digluon contribution. In the calculation we have assumed that jet misidentification probability is 1.3% (which corresponds to the ATLAS misidentification factor with a b -tagging efficiency of 60% [28]), i.e. we have multiplied the dijet cross section by a quite small number 0.013^2 . The obtained contribution is even larger than the $b\bar{b}$ one and overlays the Standard Model Higgs signal. In the case of

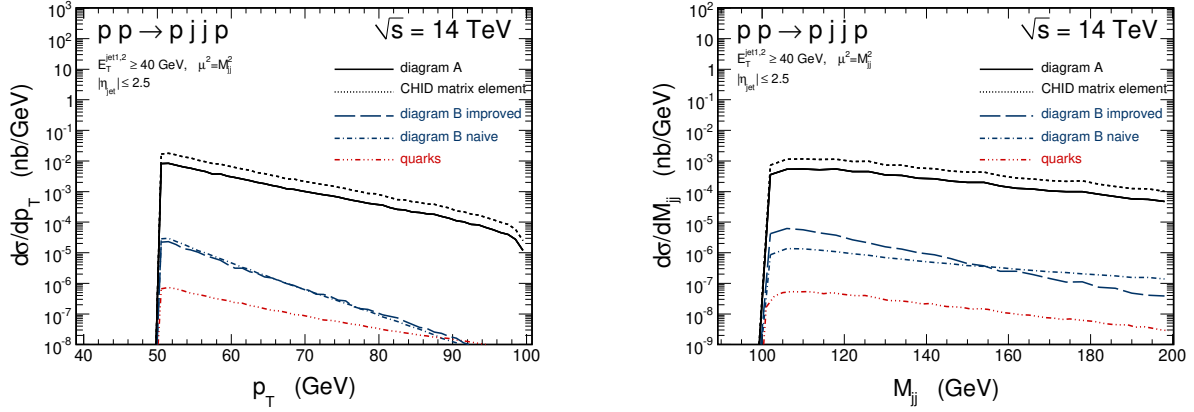


FIG. 12: The distribution in jet transverse momentum (left panel) and in dijet invariant mass (right panel).

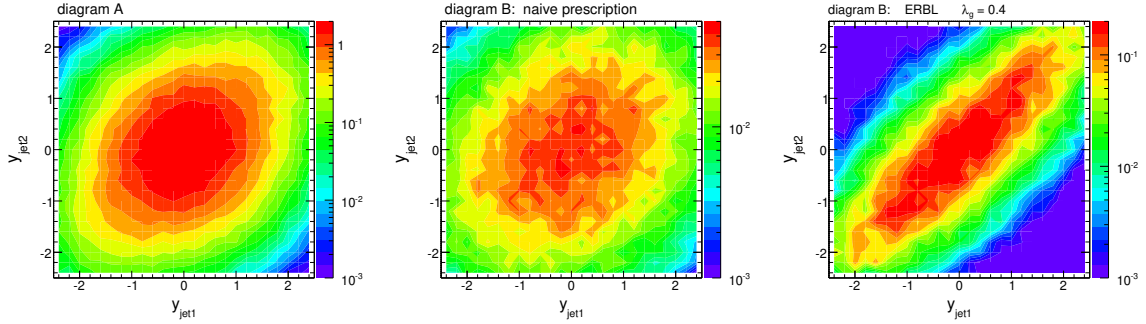


FIG. 13: $d\sigma/dy_3dy_4$ for diagram A (left panel), for diagram B, naive prescription (middle panel) and for diagram B calculated in the way proposed in this paper (right panel).

exclusive production of Higgs boson beyond the Standard Model the situation can be better (see e.g. Refs. [28, 31, 32]).

VI. CONCLUSIONS

In the present paper we have discussed the exclusive production of dijets (both digluon and quark-antiquark ones). We have included the contribution, previously known from the literature, when both gluons are emitted from the same t -channel gluon line, as well as new contributions when the gluons are emitted from different t -channel gluon lines (see Fig. 1). We have presented corresponding formulae with simple prescriptions for the unintegrated gluon distributions relevant for these two cases. For both contributions, we made predictions for various differential distributions at Tevatron (1.96 TeV) and LHC (14 TeV) energies, including an analysis of different gluon polarisation contributions and theoretical uncertainties.

The diagram B contribution turned out to be much smaller than the one (diagram A) known from the literature. They become comparable only for large rapidity differences of both jets where the cross section is rather small or when the jet transverse momenta are

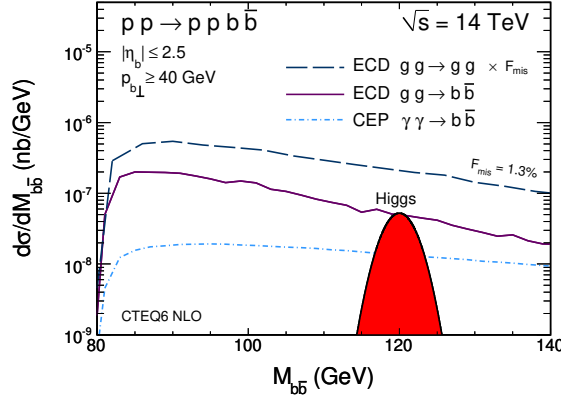


FIG. 14: Invariant mass distribution of the $b\bar{b}$ system. Shown are contributions from diffractive Higgs boson (shaded area), $b\bar{b}$ continuum (solid line), $\gamma\gamma$ continuum (dash-dotted line) and diffractive digluon contribution (dashed line) multiplied by an ATLAS misidentification factor squared.

small. The latter case can be, therefore, very important for the central diffractive production of pions. This will be discussed elsewhere.

We have found that jets corresponding to the mechanism of diagram B are strongly correlated in their rapidities. This is a consequence of a specific behavior of off-diagonal gluon distributions in the ERL region where $|x| < |\xi| \ll 1$.

We have compared our results with the CDF collaboration data. Our cross sections are somewhat larger than those obtained in the literature. Compared to those calculations, we have performed integration starting from smaller lower limit for screening gluon transverse momenta and with the choice of scale in the Sudakov form factor as advocated by Coughlin and Forshaw [3]. Our observation may mean e.g. that the gap survival probabilities are smaller than usually assumed for this process. Clearly, further work on this issue is required.

We have discussed also the dijet reducible background to the central exclusive Higgs boson production. In the framework of the same model, we have calculated the contribution of the quark-antiquark jets CEP. We have found that this contribution is much smaller than that for the gluon-gluon dijets in the whole phase space. However, the quark contribution, especially the $b\bar{b}$ one, is very important, as it constitutes an irreducible background for exclusive production of the Higgs boson. On the other hand, the gluonic jets can be misidentified as the $b\bar{b}$ jets and in this sense they also contribute to a background for exclusive production of the Higgs boson.

If both gluonic jets are misidentified as b or anti- b quark jets, then this leads to an extra background to exclusive Higgs boson production when the Higgs boson is observed in the $b\bar{b}$ decay channel. This extra contribution can be even more important than the irreducible $b\bar{b}$ contribution. When the realistic ATLAS misidentification factor is included one obtains the total background which significantly exceeds the Higgs signal. This observation suggests that the experimental observation of the exclusive Standard Model Higgs production may be very challenging. The situation may be better for beyond the Standard Model Higgs boson production though, but corresponding detailed analysis including a Monte-Carlo simulation of backgrounds still needs to be done.

Acknowledgments

We are particularly indebted to Igor Ivanov for valuable discussions on theoretical issues related to UGDFs and the Sudakov form factor. Useful discussions and helpful correspondence with Jean-Rene Cudell, Rikard Enberg, Krzysztof Golec-Biernat, Gunnar Ingelman, Valery Khoze, Alan Martin, Andy Pilkington, Christophe Royon, Mikhail Ryskin, Rafał Staszewski and Marek Tasevsky are gratefully acknowledged. This study was partially supported by the Carl Trygger Foundation and by the polish grants of MNiSW N N202 249235 and N N202 237040.

-
- [1] T. Aaltonen *et al.* [CDF Collaboration], Phys. Rev. D **77**, 052004 (2008) [arXiv:0712.0604 [hep-ex]];
A. A. Affolder *et al.* [CDF Collaboration], Phys. Rev. Lett. **88**, 151802 (2002) [arXiv:hep-ex/0109025];
A. A. Affolder *et al.* [CDF Collaboration], Phys. Rev. Lett. **85**, 4215 (2000).
 - [2] M. G. Albrow, T. D. Coughlin and J. R. Forshaw, arXiv:1006.1289 [hep-ph];
J. L. Pinfold, arXiv:1006.0204 [hep-ph].
 - [3] T. D. Coughlin and J. R. Forshaw, JHEP **1001**, 121 (2010) [arXiv:0912.3280 [hep-ph]].
 - [4] A. D. Martin, M.G. Ryskin, V.A. Khoze, Phys. Rev. **D56** (1997) 5867.
 - [5] B.E. Cox, A. Pilkington, Phys. Rev. D **72** (2005) 094024.
 - [6] J. R. Cudell, A. Dechambre, O. F. Hernandez and I. P. Ivanov, Eur. Phys. J. C **61**, 369 (2009).
 - [7] R. Maciula, R. Pasechnik and A. Szczurek, Phys. Rev. D **83**, 054014 (2011) [arXiv:hep-ph/11011439].
 - [8] R. Maciula, R. Pasechnik and A. Szczurek, arXiv:1011.5842 [hep-ph].
 - [9] A. Dechambre, O. Kepka, C. Royon and R. Staszewski, Phys. Rev. D **83**, 054013 (2011) [arXiv:1101.1439 [hep-ph]].
 - [10] R. Maciula, R. Pasechnik and A. Szczurek, Phys. Lett. B **685**, 165 (2010) [arXiv:0912.4345 [hep-ph]].
 - [11] V. S. Fadin and L. N. Lipatov, Sov. J. Nucl. Phys. **50**, 712 (1989) [Yad. Fiz. **50**, 1141 (1989)].
 - [12] V. A. Khoze, A. D. Martin and M. G. Ryskin, Phys. Lett. B **401**, 330 (1997);
A. B. Kaidalov, V. A. Khoze, A. D. Martin and M. G. Ryskin, Eur. Phys. J. C **33**, 261 (2004).
 - [13] J. R. Forshaw, arXiv:hep-ph/0508274;
J. R. Forshaw, Nucl. Phys. Proc. Suppl. **191**, 247-256 (2009). [arXiv:0901.3040 [hep-ph]].
 - [14] V. S. Fadin and L. N. Lipatov, Nucl. Phys. B **477**, 767 (1996) [arXiv:hep-ph/9602287].
 - [15] V. A. Khoze, A. D. Martin and M. G. Ryskin, Eur. Phys. J. C **19**, 477 (2001) [Erratum-ibid. C **20**, 599 (2001)] [arXiv:hep-ph/0011393].
 - [16] M.A. Kimber, A.D. Martin and M. G. Ryskin, Phys. Rev. **D63** (2001) 114027. [arXiv:hep-ph/0101348].
 - [17] A. D. Martin and M. G. Ryskin, Phys. Rev. D **64**, 094017 (2001) [arXiv:hep-ph/0107149].
 - [18] A. G. Shuvaev, K. J. Golec-Biernat, A. D. Martin and M. G. Ryskin, Phys. Rev. D **60**, 014015 (1999) [arXiv:hep-ph/9902410].
 - [19] V. A. Khoze, A. D. Martin and M. G. Ryskin, Eur. Phys. J. C **18**, 167 (2000) [arXiv:hep-ph/0007359].
 - [20] J. Pumplin, D. R. Stump, J. Huston, H. L. Lai, P. M. Nadolsky and W. K. Tung, JHEP **0207**, 012 (2002).

- [21] M. Glück, E. Reya and A. Vogt, Z. Phys. C **67**, 433 (1995).
- [22] M. Glück, D. Jimenez-Delgado, E. Reya, Eur. Phys. J. C **53**, 355 (2008).
- [23] A. D. Martin, W. J. Stirling, R. S. Thorne and G. Watt, Eur. Phys. J. C **63**, 189 (2009). [arXiv:0901.0002 [hep-ph]].
- [24] R. S. Pasechnik, A. Szczurek and O. V. Teryaev, Phys. Rev. D **78**, 014007 (2008); Phys. Lett. B **680**, 62 (2009); Phys. Rev. D **81**, 034024 (2010); Phys. Rev. **D83**, 074017 (2011); P. Lebiedowicz, R. Pasechnik, A. Szczurek, arXiv:1103.5642 [hep-ph].
- [25] A. V. Efremov, A. V. Radyushkin, Phys. Lett. **B94**, 245-250 (1980); G. P. Lepage, S. J. Brodsky, Phys. Lett. **B87**, 359-365 (1979).
- [26] P. Lebiedowicz and A. Szczurek, Phys. Rev. **D81** (2010) 036003 [arXiv:0912.0190 [hep-ph]].
- [27] W. Ochs and P. Minkowski, arXiv:1108.0589 [hep-ph].
- [28] B. E. Cox, F. K. Loebinger, A. D. Pilkington, JHEP **0710**, 090 (2007). [arXiv:0709.3035 [hep-ph]].
- [29] A. Pilkington, private communication.
- [30] Ch. Royon, private communication.
- [31] S. Heinemeyer, V.A. Khoze, M.G. Ryskin, W.J. Stirling, M. Tasevsky, and G. Weiglein, Eur. Phys. J. C **53** (2008) 231.
- [32] R. Enberg, R. Pasechnik, Phys. Rev. **D83**, 095020 (2011). [arXiv:1104.0889 [hep-ph]].
- [33] M. Chaichian, P. Hoyer, K. Huitu, V.A. Khoze, A.D. Pilkington, JHEP **0905** (2009) 011.